JOURNAL OF Materials CHEMISTRY

Ionic and p-type electronic transport in zircon-type $Ce_{1-x}A_xVO_{4\pm\delta}$ (A = Ca, Sr)†

Ekaterina V. Tsipis,[a] Mikhail V. Patrakeev,[a,b] Vladislav V. Kharton,*[a,c] Nikolai P. Vyshatko[a] and Jorge R. Frade[a]

[a]*Department of Ceramics and Glass Engineering, CICECO, University of Aveiro, 3810-193 Aveiro, Portugal. E-mail: kharton@cv.ua.pt*
[b]*Institute of Solid State Chemistry, Ural Division of RAS, 91 Pervomaiskaya Str., Ekaterinburg 620219, Russia*
[c]*Institute of Physicochemical Problems, Belarus State University, 14 Leningradskaya Str., 220050 Minsk, Republic of Belarus*

Received 21st June 2002, Accepted 12th September 2002
First published as an Advance Article on the web 23rd October 2002

Incorporation of alkaline-earth cations into the zircon-type lattice of $Ce_{1-x}A_xVO_4$ (A = Ca, Sr; x = 0–0.2) leads to higher p-type electronic conductivity, while the tetragonal unit cell volume and Seebeck coefficient decrease due to increasing concentration of electron holes localised on cerium cations. The oxygen ion transference numbers of $Ce_{1-x}Ca_xVO_4$ in air, determined by faradaic efficiency measurements, vary in the range from 2×10^{-4} to 6×10^{-3} at 973–1223 K, increasing with temperature. The ionic conductivity is essentially independent of calcium content and decreases with reducing oxygen partial pressure. The activation energy for ionic transport in $Ce(Ca)VO_4$ is 90–125 kJ mol^{-1}. Doping with calcium enhances the stability of cerium orthovanadate at reduced oxygen pressures, shifting the phase decomposition limits down to oxygen activity values of 10^{-16}–10^{-14} atm at 1023 K. The results on structure, Seebeck coefficient, and the partial p-type electronic and oxygen ionic conductivities suggest the presence of hyperstoichiometric oxygen in the $Ce_{1-x}A_xVO_{4+\delta}$ lattice. The hyperstoichiometry, estimated from Seebeck coefficient data in the $p(O_2)$ range from 10^{-19} to 0.75 atm at 923–1223 K, may achieve 2–3% of the total oxygen content and weakly depends on the temperature and oxygen pressure variations within the zircon phase existence domain. Thermal expansion coefficients of $Ce_{1-x}A_xVO_{4+\delta}$ ceramics in air, calculated from dilatometric data, are in the narrow range (5.6–5.9) $\times 10^{-6}$ K^{-1} at 400–800 K.

1. Introduction

Oxide phases of the ternary system Ce–V–O attract substantial attention due to their unique optical, catalytic, electrical and magnetic properties.[1–6] Potential applications of these oxides include counter electrodes in electrochromic devices, oxidation catalysts, luminescent materials and sensors. One of the most interesting compounds in the Ce–V–O system is cerium orthovanadate, $CeVO_4$, which has a tetragonal zircon-type structure (space group $I4_1/amd$) and stabilises Ce^{3+} cations even in oxidising conditions.[1–3,7–10] The dominant trivalent state of cerium ions in the lattice of $CeVO_4$ in air was proven by X-ray absorption spectroscopy (XAS)[9] and thermogravimetric analysis (TGA),[7] though the results of both experiments cannot exclude the presence of minor fractions of Ce^{4+}, as suggested in ref. 10. No essential changes in the oxygen stoichiometry were detected by TGA in the temperature range 300–1270 K.[10] At temperatures in the region of 1173 K, a transformation of the zircon- into scheelite-type phase of $CeVO_4$ was suggested to explain the conductivity behaviour and the results of differential thermal analysis (DTA).[10] The total conductivity of cerium orthovanadate is predominantly p-type electronic, with an activation energy of approximately 36 kJ mol^{-1}; the oxygen ionic contribution at temperatures up to 1073 K was found to be lower than the detection limit of the emf method.[7] As a possible mechanism of the electron-hole transport, hopping between Ce^{4+} and Ce^{3+} ions was suggested for the temperature range 400–680 K.[10] The conductivity can be considerably enhanced by substitution of cerium with divalent metal cations, such as Ca, Sr or Pb; the highest conductivity values in air were reported for the compositions $Ce_{0.8}Ca_{0.2}VO_4$ and $Ce_{0.9}Sr_{0.1}VO_4$.[7]

It should be mentioned that binary oxides of both cerium and vanadium exhibit high catalytic activity in reactions involving oxygen and are thus used as the components of electrode materials in solid oxide fuel cells (SOFCs).[11–15] In particular, the incorporation of ceria into SOFC anodes, where most cerium cations are reduced to Ce^{3+}, leads to a considerable improvement in the SOFC performance.[12,13,15] Therefore, $CeVO_4$-based phases having a high catalytic activity[4] and a significant conductivity[7] might be of interest for high-temperature electrochemical applications, provided that they offer sufficient stability under the operation conditions. Although in the binary V–O system the reduction of V^{5+} occurs at relatively high oxygen pressures,[16,17] pentavalent vanadium cations are more stable in multicomponent oxide compounds, such as alkaline-earth and rare-earth vanadates.[4,17]

The present work is focused on the study of transport and physicochemical properties of $Ce_{1-x}A_xVO_4$ (A = Ca, Sr; x = 0–0.2). Particular emphasis is given to properties determining applicability in high-temperature electrochemical cells, including the partial oxygen ionic and electronic conductivities, thermal expansion, and phase stability limits at reduced oxygen pressures. In order to reveal mechanisms of ionic and electronic transport, the total conductivity and Seebeck coefficient of $Ce(A)VO_4$ were studied as functions of the oxygen partial pressure.

†Electronic supplementary information (ESI) available: oxygen partial pressure dependence of the total conductivity and Seebeck coefficient of $Ce_{0.8}Ca_{0.2}VO_{4+\delta}$ (Fig. S1) and of the electron-hole mobility in $Ce_{1-x}Ca_xVO_{4+\delta}$ at 1023 K (Fig. S2). See http://www.rsc.org/suppdata/jm/b2/b206004c/

 DOI: 10.1039/b206004c

Table 1 Properties[a] of $Ce_{1-x}A_xVO_4$ ceramics

Composition	d_{exp}/g cm^{-3}	d_{exp}/d_{theor} (%)	$\bar{a} \times 10^6$/K^{-1} (400–800 K)	Activation energy for the total conductivity in air (400–1200 K)		$q \times 10^{20}$/J
				E_a/kJ mol^{-1}	ln A_0/S K cm^{-1}	
$CeVO_4$	4.73	99	5.64 ± 0.01	37.9 ± 0.8	7.9 ± 0.1	4 ± 1
$Ce_{0.9}Ca_{0.1}VO_4$	4.34	93	5.89 ± 0.01	35.2 ± 0.6	9.8 ± 0.1	2.0 ± 0.3
$Ce_{0.8}Ca_{0.2}VO_4$	4.39	97	5.64 ± 0.01	34.6 ± 0.7	9.2 ± 0.1	1.8 ± 0.2
$Ce_{0.9}Sr_{0.1}VO_4$	4.44	95	5.73 ± 0.01	34.8 ± 0.5	9.32 ± 0.08	–

[a] d_{exp} and d_{theor} are the experimental and theoretical density values, respectively. $\bar{a}$ is the linear thermal expansion coefficient (TEC) in air, averaged in the temperature range 400–800 K. E_a and A_0 are the regression parameters of the Arrhenius model for the total conductivity. q is the transported heat of electron holes, calculated from the temperature dependences of Seebeck coefficient in air (see text).

2. Experimental

Single-phase powders of $CeVO_4$, $Ce_{0.9}Sr_{0.1}VO_4$ and $Ce_{1-x}Ca_xVO_4$ ($x = 0.1$ and 0.2) were synthesised using a standard ceramic technique from stoichiometric amounts of $Ce(NO_3)_3 \cdot 6H_2O$ (Aldrich), V_2O_5 (Fluka), $SrCO_3$ (BDH) and $CaCO_3$ (Fluka); for all starting materials the purity was not less than 99%. Solid-state reactions were conducted in air at 770–1070 K for 20–30 h with multiple intermediate regrindings. Formation of single zircon-type phases was verified by X-ray diffraction (XRD) analysis. The disk- (diameter of 10–15 mm) and bar-shaped ($4 \times 4 \times 30$ mm^3) samples were compacted from ball-milled powders at 200–350 MPa; sintering of gas-tight ceramics was performed in air at 1420–1650 K during 2–8 h with subsequent slow cooling, in order to achieve equilibrium with air at room temperature. Characterisation of the ceramic materials included XRD, scanning electron microscopy combined with energy dispersive spectroscopy (SEM-EDS), TGA-DTA, and dilatometry. Structure refinement was performed using the Fullprof program;[18] the Ce/A sites were assumed fully disordered. TGA was carried out using a Linseis L70/2001 apparatus in atmospheric air and a Setaram LabSys TG-DTA16 instrument in a flow of high-purity nitrogen or oxygen. The total electrical conductivity in air was measured at 300–1300 K by 4-probe dc technique, van der Pauw method and ac impedance spectroscopy. Combined measurements of the total conductivity and Seebeck coefficient as functions of the oxygen partial pressure were performed in a cell with two separated samples at 1023–1223 K in the $p(O_2)$ range from 10^{-19} to 0.75 atm. The experimental techniques and equipment used for the characterisation and electrical measurements, are described elsewhere (refs. 19–24 and references cited therein). The values of the oxygen ion transference numbers and ionic conductivity were calculated from the results of faradaic efficiency and total conductivity. A detailed description of the faradaic efficiency measurement technique can be found in refs. 20 and 21. These measurements were carried out at 973–1223 K, either under zero oxygen chemical potential gradient in atmospheric air or under the oxygen pressure gradient of 0.21/0.13 atm. In the latter case, the results were corrected for the steady oxygen permeation fluxes, independently measured prior to the faradaic efficiency determination.[21]

3. Results and discussion

3.1. Materials characterisation

XRD studies showed that, as for the synthesised powders, sintered ceramic samples of $Ce_{1-x}A_xVO_4$ were single phase. Density of the ceramics was no less than 93% of their theoretical density calculated from XRD results (Table 1). SEM-EDS analysis detected no phase impurities; SEM micrographs reflecting microstructures typical for the $Ce(A)VO_4$ ceramics are presented in Fig. 1. The average grain size was similar for all materials, varying in the range 7–20 μm. Although some traces of liquid phase formation were observed at the grain boundaries, cation composition of the ceramic materials was

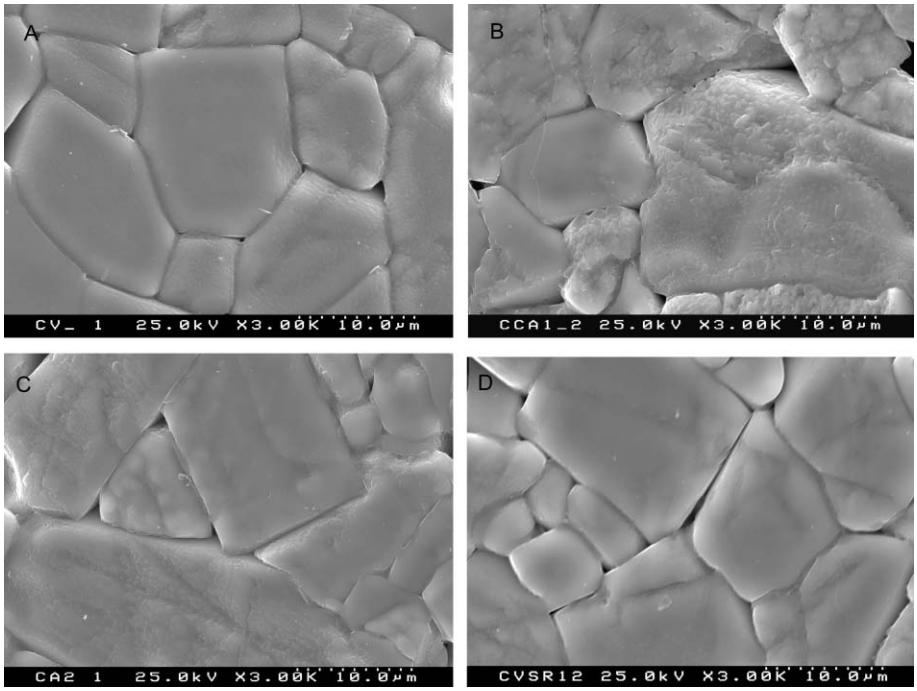

Fig. 1 SEM micrographs of zircon-type ceramics: $CeVO_4$ (A), $Ce_{0.9}Ca_{0.1}VO_4$ (B), $Ce_{0.8}Ca_{0.2}VO_4$ (C), and $Ce_{0.9}Sr_{0.1}VO_4$ (D).

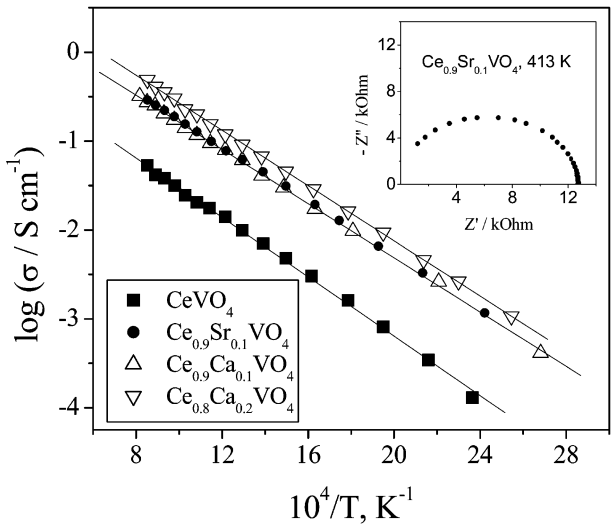

Fig. 2 Temperature dependence of the total conductivity of $Ce_{1-x}A_xVO_4$ ceramics in air. Inset shows an example of the typical impedance spectra for $Ce_{0.9}Sr_{0.1}VO_4$.

found to be uniform within the limits of experimental error. Impedance spectroscopy confirmed a negligible effect of the grain boundaries on the conductivity; an example of typical impedance spectra is shown in the inset of Fig. 2.

The average thermal expansion coefficients (TECs) of $Ce_{1-x}A_xVO_4$, calculated from dilatometric data collected in air, vary in the very narrow range (5.6–5.9) $\times$ 10^{-6} K^{-1} at 400–800 K (Table 2). At these temperatures, the thermal expansion of $Ce_{1-x}A_xVO_4$ ceramics is almost linear. Anomalous results with near zero expansion were observed in the dilatometric curves around 850–1100 K. Such a behaviour has been previously observed for several $LaGaO_3$-based phases[25] and was discussed in terms of phase transitions. Indeed, the DTA curves exhibited a broad endothermic effect at temperatures 1070–1120 K, in agreement with the literature.[10] However, XRD analysis of $CeVO_4$ samples, annealed in air at 1173 K and then quenched in liquid nitrogen, showed that the zircon-type phase undergoes no transitions in this temperature range. This conclusion was confirmed by high-temperature XRD studies at 300–1273 K. The results on electrical properties, presented below, are therefore related to single zircon-type phases; more detailed studies are necessary to reveal the exact reasons for the anomalous TEC behaviour.

3.2. Crystal structure

The tetragonal unit cell parameters, *a* and *c*, of zircon-type $Ce_{1-x}A_xVO_4$ are listed in Table 2. Tetragonal distortion of the lattice, expressed by the *a*/*c* ratio, decreases when cerium is substituted for either calcium or strontium. Doping with alkaline-earth cations also leads to decreasing unit cell volume, in agreement with literature data.[7,8] It should be noted that the ionic radius of 8-coordinated Ce^{3+} is similar to that of Ca^{2+}

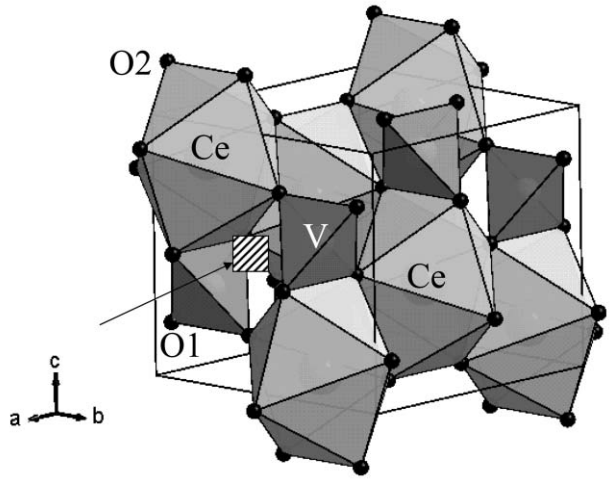

Fig. 3 Zircon-type structure of $Ce_{1-x}A_xVO_{4+\delta}$. The square shows the most probable position of hyperstoichiometric oxygen.

and is smaller than the radius of strontium.[26] The decrease in the lattice parameters may therefore suggest that cerium substitution induces the formation of Ce^{4+} cations, the size of which is considerably smaller than other ions occupying Ce sites.[26] In order to estimate the oxidation states of cerium and vanadium, the cation–anion distances were calculated from the structure refinement results (Table 2). In the case of Ce ions, the existence of two non-equivalent oxygen positions in the lattice (O1 and O2, Fig. 3) results in two different Ce–O distances; the average bond length values were taken for the estimations.

The interatomic distances V–O, determined from the refinement data, were found to be similar to those estimated as the sum of O^{2-} and 4-coordinated V^{5+} radii,[26] suggesting that the predominant oxidation state of vanadium is 5+. For Ce–O bonds, however, the average length is smaller than that expected for Ce^{3+}–O^{2-}, but greater than estimated for Ce^{4+}–O^{2-}. Again, this might indicate the presence of a significant fraction of tetravalent cerium cations in the lattice. The fraction of Ce^{4+}, calculated assuming the Ce–O bond length to be the sum of average Ce-site cation and oxygen anion radii,[26] increases from 13 to 33% with increasing dopant content (Table 2). The oxygen nonstoichiometry of $(Ce^{3+}_{1-y}Ce^{4+}_{y})_{1-x}A_xVO_{4\pm\delta}$ is related to cerium oxidation state *via* the electroneutrality condition:

$$\delta = \frac{y - x - xy}{2} \quad (1)$$

where *y* is the fraction of Ce^{4+}. Calculations of the oxygen content showed that all title materials are possibly oxygen-hyperstoichiometric; the estimated δ values vary in the range from +0.03 to +0.08 at room temperature (Table 2). Although these estimations are very crude, the assumptions regarding oxygen hyperstoichiometry and increasing cerium oxidation state on doping are in agreement with the results on the total

Table 2 Structure refinement results[a] of $Ce_{1-x}A_xVO_{4+\delta}$ at room temperature

Composition	Unit cell parameter			Average bond lengths/Å		Fraction (*y*) of Ce^{4+} (%)	δ
	a/Å	*c*/Å	*V*/Å^3	Ce–O	V–O		
$CeVO_4$	7.396(8)	6.496(9)	355.5	2.52	1.66	13	0.07
$Ce_{0.9}Ca_{0.1}VO_4$	7.354(0)	6.472(0)	350.0	2.49	1.68	30	0.08
$Ce_{0.8}Ca_{0.2}VO_4$	7.314(5)	6.450(9)	345.1	2.49	1.64	33	0.03
$Ce_{0.9}Sr_{0.1}VO_4$	7.381(0)	6.491(5)	353.7	2.52	1.68	24	0.06

[a] *V* is the unit cell volume. The Ce–O bond lengths were averaged between Ce–O1 and Ce–O2 interatomic distances. *y* is the fraction of Ce^{4+}, estimated from the bond length values and multiplied by 100%. δ is the oxygen hyperstoichiometry calculated from *y* using the crystal electroneutrality law.

Table 3 Parameters of the oxygen ion transport in $Ce_{1-x}Ca_xVO_{4+\delta}$ in air

	Average ion transference numbers[a]		Activation energy for ionic conductivity[b]	
Composition	T/K	t_o	T/K	E_a/kJ mol^{-1}
$CeVO_{4+\delta}$	1223	5.6×10^{-3}	973–1123	124 ± 9
	1173	4.1×10^{-3}	1123–1223	92 ± 10
	1123	4.2×10^{-3}		
	1073	2.5×10^{-3}		
	1023	1.4×10^{-3}		
	973	1.1×10^{-3}		
$Ce_{0.8}Ca_{0.2}VO_{4+\delta}$	1223	7.3×10^{-4}	973–1223	90 ± 6
	1173	5.5×10^{-4}		
	1123	3.9×10^{-4}		
	1073	3.0×10^{-4}		
	1023	2.5×10^{-4}		
	973	2.0×10^{-4}		

[a]Each t_o value was averaged from 2–4 experimental data points. [b]The oxygen ionic conductivity was calculated from the results on the total conductivity and transference numbers, determined by the faradaic efficiency method, as $\sigma_0 = \sigma \times t_o$.

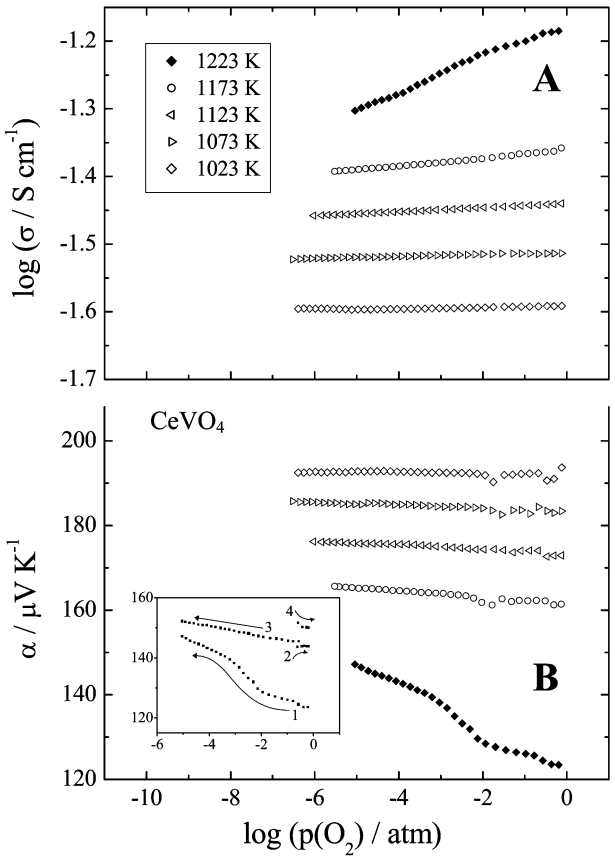

Fig. 4 Oxygen partial pressure dependence of the total conductivity (A) and Seebeck coefficient (B) of $CeVO_{4+\delta}$. Inset illustrates irreversible behaviour of the thermopower after phase decomposition, with the numbers and arrows showing the sequence of the oxygen pressure changes.

electrical conductivity, Seebeck coefficient, and partial ionic conductivity of $Ce_{1-x}A_xVO_{4+\delta}$, as discussed below.

Finally, the structure of $CeVO_4$ was analysed to locate the positions available for hyperstoichimetric oxygen. Incorporation of the extra oxygen ions into either V–O tetrahedra or Ce–O dodecahedra constituting the zircon-type lattice (Fig. 3) seems unlikely. Such an incorporation would lead to an increase in the bond lengths due to increasing cation coordination numbers, which contradicts the refinement results (Table 2).

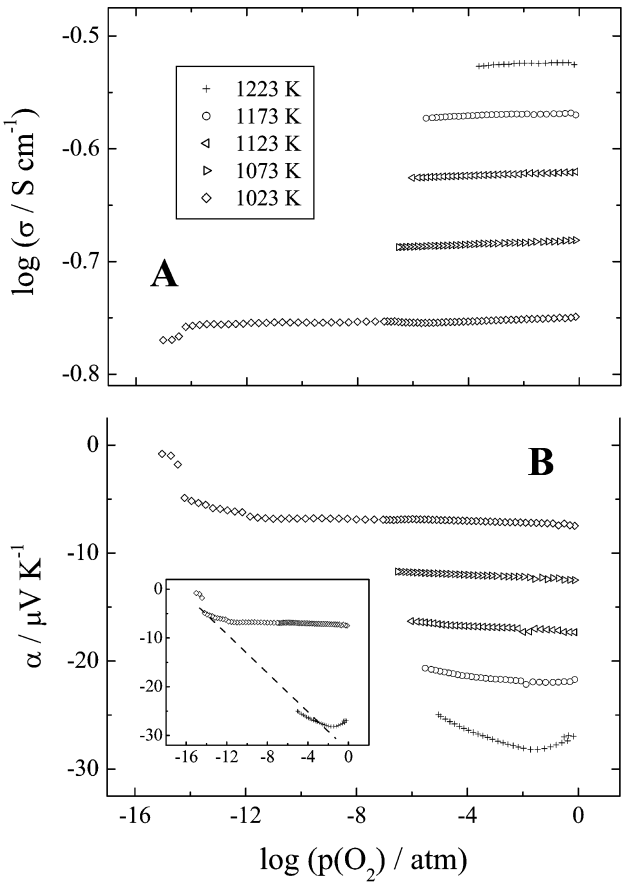

Fig. 5 Oxygen partial pressure dependence of the total conductivity (A) and Seebeck coefficient (B) of $Ce_{0.9}Ca_{0.1}VO_{4+\delta}$. Inset illustrates the estimation of the phase stability boundary from the thermopower data.

The most likely location of a hyperstoichiometric anion is to be found in a void between two V–O tetrahedra, marked by the square in Fig. 3. These voids form 1/2 an additional oxygen site per formula unit of $CeVO_{4+\delta}$; the hypothetical maximum oxygen nonstoichimetry of cerium orthovanadate, satisfying the lattice conservation condition, corresponds thus to the value of $\delta = +0.5$.

3.3. Total conductivity and Seebeck coefficient

The temperature dependence of the total conductivity (σ) of $Ce_{1-x}A_xVO_{4+\delta}$ ceramics in air is presented in Fig. 2. The conductivity values obtained by the different techniques, including 4-probe dc and van der Pauw methods and ac impedance spectroscopy, were found to be equal within the limits of experimental uncertainty and very similar to the literature data,[7] thus confirming the reliability of the results. Faradaic efficiency measurements showed that the ionic contribution to the total conductivity of $Ce(A)VO_{4+\delta}$ is very small; the oxygen ion transference numbers (t_o) at 973–1223 K in air are less than 0.006 (Table 3). The values of the activation energy (E_a) for electronic conduction, calculated by the standard Arrhenius equation

$$\sigma = \frac{A_0}{T}\exp\left[-\frac{E_a}{RT}\right] \quad (2)$$

where A_0 is the pre-exponential factor, are listed in Table 1. The activation energy varies in the range 34–38 kJ mol^{-1}, slightly decreasing when dopant concentration increases.

Reducing oxygen partial pressure leads to decreasing total conductivity of $Ce_{1-x}A_xVO_{4+\delta}$, whilst the values of Seebeck coefficient were found to increase (see Figs. 4 and 5 and ESI).

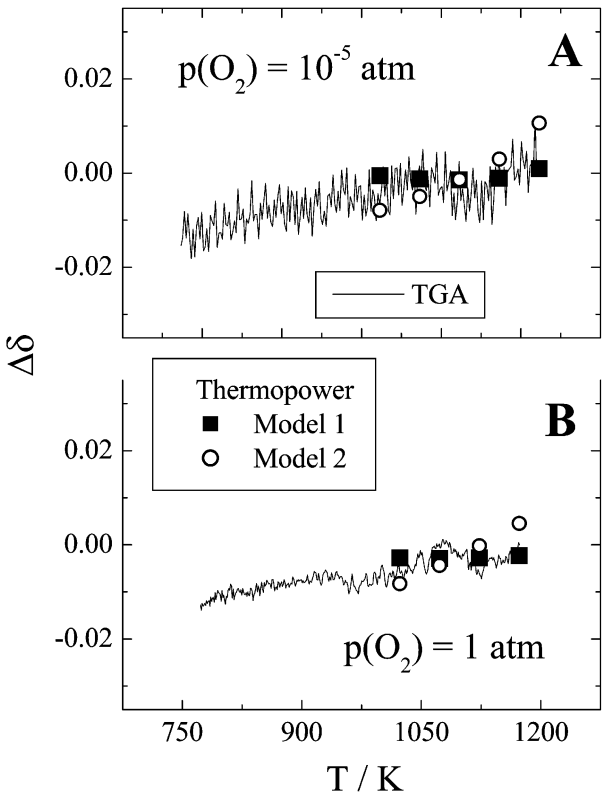

Fig. 6 Oxygen nonstoichiometry variations in $CeVO_{4+\delta}$, estimated from TGA and Seebeck coefficient data.

Within the phase stability limits, these changes are relatively small: for example, the slope of σ *vs.* $p(O_2)$ logarithmic dependences is as low as 5×10^{-4}–3×10^{-2}. Such a behaviour is due to minor oxygen content variations in the studied range of temperatures and oxygen pressures, confirmed by TGA studies in atmospheres with various $p(O_2)$. In agreement with ref. 10, the changes in δ values with temperature, determined by TGA, are comparable with the experimental error; an example is given in Fig. 6. The oxygen nonstoichiometry variations on changing oxygen pressure were also small, close to the level of experimental uncertainty.

Further decrease in $p(O_2)$ results in the decomposition of the zircon-type phases, which is associated with an irreversible drop in the conductivity and a poor reproducibility of the results; the decomposition phenomena are illustrated by insets in Figs. 4B and 5B. Although the stability limit of undoped $CeVO_4$ at 1223 K is quite close to the atmospheric oxygen pressure, the time-independent conductivity of cerium vanadate in air (see ESI) suggests an absence of phase changes, in agreement with XRD results.

Possible mechanisms of the electronic conduction in $Ce_{1-x}A_xVO_{4+\delta}$ are briefly discussed below. Generally, one can note that both the sign of Seebeck coefficient and the oxygen pressure dependences of thermopower and conductivity of $CeVO_{4+\delta}$ (Fig. 4) unambiguously indicate the dominating role of electron holes in the charge-transfer processes. Such a conclusion corresponds well to the literature data.[7,10] Doping with calcium leads to a change in the sign of the Seebeck coefficient, which becomes negative (Fig. 5 and ESI); the type of $p(O_2)$ dependences of the electrical properties remains, however, similar to that of undoped cerium orthovanadate. As shown below, this behaviour results, most likely, from increasing hole concentration and cannot be attributed to a transition from p- to n-type conduction. The conductivity enhancement on acceptor-type doping also confirms that the p-type electronic conduction prevails.

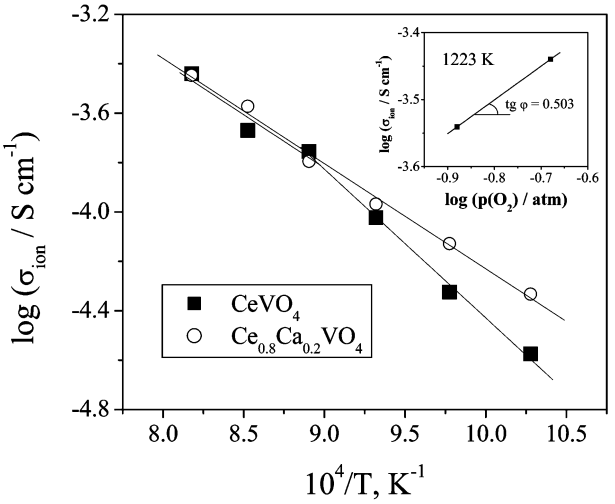

Fig. 7 Temperature dependence of the oxygen ionic conductivity of $Ce_{1-x}Ca_xVO_{4+\delta}$ ceramics in air. Inset shows the ionic conductivity of $CeVO_{4+\delta}$ as a function of the membrane permeate-side oxygen pressure, with feed-side $p(O_2)$ fixed at 0.21 atm.

3.4. Ionic transport

Fig. 7 presents the temperature dependence of the oxygen ionic conductivity of $Ce_{1-x}Ca_xVO_{4+\delta}$ ceramics, calculated from the results of the faradaic efficiency and total conductivity measurements in air. At temperatures above 1100 K, the ionic conductivity of $Ce_{0.8}Ca_{0.2}VO_{4+\delta}$ is very close to that of undoped cerium vanadate; the activation energy values are 90–92 kJ mol^{-1} (Table 3). At lower temperatures, $CeVO_{4+\delta}$ exhibits a higher activation energy and a slightly lower ionic conductivity with respect to $Ce_{0.8}Ca_{0.2}VO_{4+\delta}$ ceramics. The increase in the ionic transport in undoped cerium vanadate at $T > 1100$ K may be associated with a minor increase in the oxygen content, as shown by TGA (Fig. 6), or with partial disordering in the oxygen sublattice on heating. The latter phenomenon is quite typical for various oxide materials (*e.g.* refs. 15 and 22, and references cited therein). The oxygen ion transference numbers at 973–1223 K vary in the range (1–6) $\times$ 10^{-3} for $CeVO_{4+\delta}$ and (2–8) $\times$ 10^{-4} for $Ce_{0.8}Ca_{0.2}VO_{4+\delta}$.

As illustrated by the inset in Fig. 7, the ionic conduction in $CeVO_{4+\delta}$ decreases with reducing oxygen pressure, suggesting an oxygen interstitial diffusion mechanism. In the case of a vacancy mechanism, an increase in σ_{ion} with decreasing $p(O_2)$ might be expected. The slope of σ_{ion} dependence on the membrane permeate-side oxygen pressure is close to 0.5, which may indicate that the overall ionic transport is limited by the concentration of oxygen interstitials at the permeate-side surface. Notice also that the interstitial migration mechanism, with preferable diffusion between the chains along the *c* axis of the zircon-type lattice, was recently proposed for the explanation of transport properties of $EuVO_4$.[27]

The similar values of the ionic conductivity in $Ce_{1-x}Ca_xVO_{4+\delta}$ (x = 0–0.2) can be considered as further evidence of the interstitial ion migration, supporting the hypothesis of non-negligible oxygen hyperstoichiometry in the title materials. Indeed, if cerium vanadate was nearly stoichiometric with the prevailing charge compensation mechanism *via* the oxygen vacancy formation,[7–9] a systematic increase in the ionic conduction should be expected due to increasing vacancy concentration when calcium content increases. One typical example of such behaviour refers to acceptor-doped perovskites, such as Mg-containing $Sr(Ti,Fe)O_{3-\delta}$ phases,[21] where incorporation of lower-valence cations leads to increasing ionic conductivity, almost proportional to the induced oxygen hypostoichiometry. Therefore, the observed behaviour (Fig. 7)

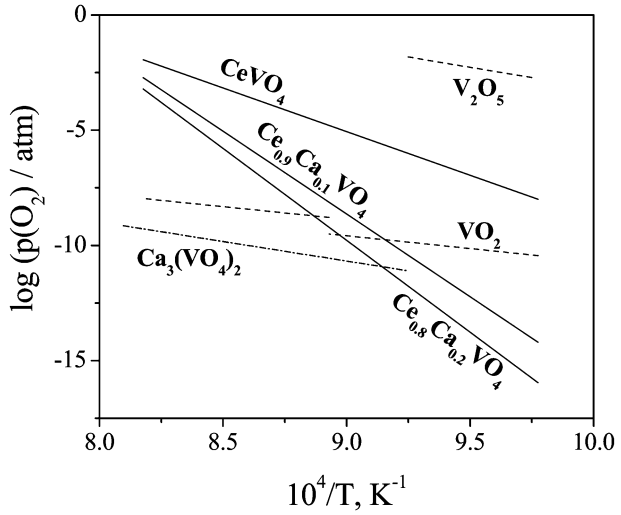

Fig. 8 Phase stability limits of $Ce_{1-x}Ca_xVO_{4+\delta}$. Literature data on binary vanadium oxides[16,29] and $Ca_3(VO_4)_2$[30] are shown for comparison.

should be rather attributed to predominant interstitial diffusion due to the presence of hyperstoichiometric oxygen in the lattice, with negligible vacancy contribution. Calcium charge compensation seems to occur mainly *via* formation of electron holes located on Ce cations, which has no essential effect on the anion charge carrier concentration. It should be mentioned that the coexistence of oxygen vacancies and interstitials in $Ce_{1-x}Ca_xVO_{4+\delta}$ lattice with an intrinsic Frenkel-type equilibrium, like La_2NiO_4-based phases,[28] cannot be excluded. In this case, whilst doping with calcium would shift the equilibrium towards oxygen vacancy formation, similar values of σ_{ion} of the compositions with $x = 0$ and 0.2 at $T > 1100$ K would indicate a dominant interstitial diffusion mechanism.

3.5. Stability

The low-$p(O_2)$ stability limits of zircon-type $Ce_{1-x}Ca_xVO_{4+\delta}$ were evaluated from the oxygen partial pressure dependences of the total conductivity and Seebeck coefficient; an example is shown in the inset of Fig. 5B. In Fig. 8 these phase boundaries are combined with the thermodynamic data on binary vanadium oxides and calcium vanadate.[16,29,30] Decomposition of undoped $CeVO_{4+\delta}$ was found to occur at oxygen partial pressures below the stability boundary of $V_2O_{5-\delta}$ and nearly in the center of the stability domain of VO_2-based phase; this confirms the observation[4] that cerium orthovanadate is less reducible than pure V_2O_5, possibly due to structural reasons. Note that the ionic radius of V^{4+} is clearly larger than that required to maintain the tetrahedral coordination in cerium orthovanadate. On the contrary, reducing conditions should stabilise the expected valence state of cerium in the zircon-type lattice, Ce^{3+}. An extrapolation of the $CeVO_{4+\delta}$ stability boundary towards higher temperatures and higher $p(O_2)$ indicates that in atmospheric air cerium orthovanadate may decompose at temperatures around 1250–1300 K. However, as mentioned above, no further evidence of phase transformations in air was observed by XRD.

Doping with calcium leads to a considerable enlargement of the zircon phase stability domain, which is associated most probably with an increase in the concentrations of ionic species with higher valence states at a given value of $p(O_2)$. One thus expects that Ca doping increases the concentration of Ce^{4+} and suppresses the formation of V^{4+}. In fact, the decomposition of $Ce_{1-x}Ca_xVO_{4+\delta}$ takes place at values of $p(O_2)$ of 10^{-16}–10^{-8} atm at 1020–1100 K, which are comparable to the stability boundaries of VO_2 and $Ca_3(VO_4)_2$. The ability to retain the highest oxidation state (V^{5+}) is thus enhanced by the tetrahedral coordination of vanadium cations in cerium orthovanadate and by additions of calcium, as observed in alkaline-earth vanadates.[17,30] Notice also that extrapolation of the stability limit of $Ce_{0.8}Ca_{0.2}VO_{4+\delta}$ to the low-temperature range suggests that this phase should be stable in the SOFC anode environments at temperatures below 950 K, when the decomposition is expected at $p(O_2) < 10^{-20}$ atm.

Some authors[4] reported that the decomposition of cerium orthovanadate may proceed by a single step conversion to a $CeVO_3$ phase. In fact, vanadium and cerium are both trivalent in the latter compound, and the stability limit of $CeVO_{4+\delta}$ is close to the VO_2–V_2O_3 phase boundary, corresponding to the reduction of vanadium cations to the dominant oxidation state of 3+. In spite of these observations, further studies are required to interpret other findings and to understand the decomposition mechanisms of $CeVO_4$-based materials. For example, XRD analysis of $CeVO_4$ annealed in a flow of 10% H_2–90% N_2 mixture at 923 K showed the formation of Ce_2O_3 or $CeO_{2-\delta}$, without traces of $CeVO_3$. Similar results were obtained under vacuum (with oxygen partial pressure of about 2×10^{-9} atm) where only reflections of $CeO_{2-\delta}$ were observed in the XRD patterns. Substitution of cerium with alkaline-earth cations can be accommodated by the lattice as it has no essential effect on the average radius of vanadium cations, the oxidation state of which is predominantly 5+. Another conclusion is that the decomposition mechanism of cerium orthovanadate at low $p(O_2)$ is more complicated than a one-step conversion of $CeVO_4$ into $CeVO_3$; decreasing oxygen content in the lattice seems to result in the formation of Ce-deficient zircon-type solid solutions. Detailed studies of the decomposition reactions are now in progress.

3.6. Evaluation of p-type conduction mechanism

The effect of the oxygen pressure variations on the total conductivity and Seebeck coefficient (Figs. 4 and 5 and ESI) was found to be much weaker than the influence of Ca doping and temperature. A Jonker-type analysis[31] of these data unambiguously shows that the title materials are extrinsic p-type semiconductors. In particular, all α–$\ln(\sigma)$ isotherms presenting various combinations of the data points with one fixed parameter, such as $p(O_2)$ or x, have a negative slope comparable to $(-k/e)$. A similar conclusion on the conduction type can be drawn when separately considering the dependences of α *vs.* $p(O_2)$, α *vs.* T, and σ *vs.* $p(O_2)$.[32,33] Furthermore, the shape of the Jonker-type curves (Fig. 9) is characteristic of p-type small-polaron transport.[34] Taking into account literature data[32] which show that electronic conduction in both cerium and vanadium oxides occurs *via* hopping mechanisms, a small polaron conduction in $Ce_{1-x}A_xVO_{4+\delta}$ seems quite

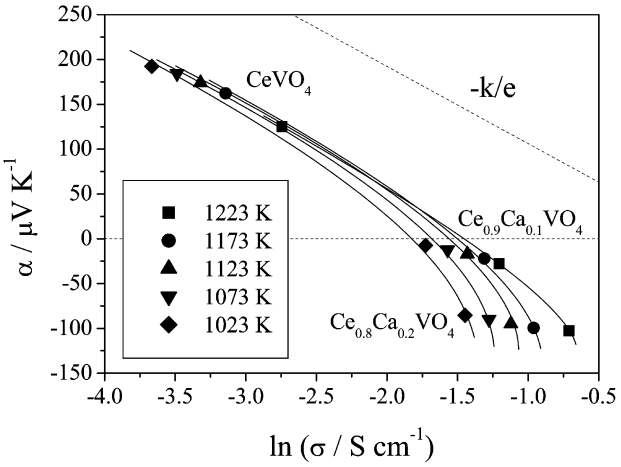

Fig. 9 Seebeck coefficient of $Ce_{1-x}Ca_xVO_{4+\delta}$ in air, plotted *vs.* corresponding conductivity values.

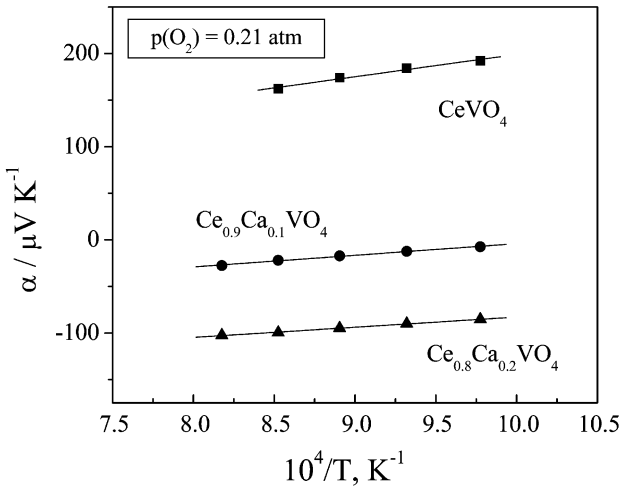

Fig. 10 Temperature dependence of the Seebeck coefficient of $Ce_{1-x}Ca_xVO_{4+\delta}$ in air.

likely. Note also that attempts to estimate the ratio between the density of states (N_p) and hole concentration (p) using a simple narrow-band approach[33] resulted in unreasonable values ($p > N_p$), whereas the low electron-hole mobility presented below is consistent with a small-polaron model.[32–34]

For a hopping mechanism, the Seebeck coefficient (α) can be expressed as[31–37]

$$\alpha = \frac{k}{e}\left(\ln\frac{N-\beta p}{p} + \frac{q}{kT}\right) \quad (3)$$

where p is the hole concentration, N is the total concentration of sites participating in the conduction process, q is the transported heat of the holes, and β is the blocking factor, which renders a fraction of the sites neighbouring a charge carrier unavailable for occupancy. The transported heat, q, which can be estimated from the temperature dependences of the thermopower at fixed carrier concentration,[36] is often neglected.[33,34,37] Table 1 lists the estimates of q in air; the corresponding Seebeck coefficient data are shown in Fig. 10.

Evaluation the p/N ratio by eqn. (3) show that more than half of sites, available for hopping in the lattice of $Ce_{1-x}Ca_xVO_{4+\delta}$, are occupied. For example, at $\beta = 1$ these estimates in air increase from 0.61 ($x = 0$) up to 0.91 ($x = 0.2$). For moderate p/N values observed at $x = 0$, the negative concentration-dependent part of eqn. (3) is compensated by the transported heat of the holes, positive by definition.[33] Increasing calcium content leads to a greater p/N ratio and, hence, a lower Seebeck coefficient, which becomes negative at $x \geqslant 0.1$. At the same time, the dominant oxidation state of vanadium in these conditions is 5+;[7,16,17,29] in vanadate-based oxide compounds the V^{5+} cations contribute, as a rule, to n-type electronic transport.[10,37,38] The hole conduction is provided, therefore, by the cerium sublattice. However, the existence of 60–90% tetravalent cerium would contradict significantly the results on crystal structure, discussed above, and the XAS and TGA data.[7,9] This suggests either blocking of part of the cerium sites, or a more complex conduction mechanism. In the course of analysis of the transport processes, more than 10 different defect/conduction models were examined; the results of the two simplest models, considered as qualitatively reasonable, are given in Table 4 and in the ESI. For the small-polaron approach, very weak variations in the hole concentration with temperature are determined by small changes in the oxygen content, in agreement with TGA (Fig. 6); no temperature activation of the charge carriers was assumed.

The first model, hereafter referred to as Model 1, is based on the assumption that each hole is located on a cerium cation and blocks the nearest Ce sites. In the zircon structure (Fig. 3), the number of such nearest neighbours is 4. Combinatorial analysis shows two possible limiting cases. For small hole concentrations ($p \ll N$), $\beta = 5$. When hole concentration is maximum ($p \rightarrow 0.5\ N$), $\beta = 2$. Assuming that β is a linear function of p between these limiting cases, one can obtain

$$\frac{p}{N} = \frac{1}{6}(\beta - 2) \quad (4)$$

Substitution of eqn. (4) into eqn. (3) with subsequent fitting of the Seebeck coefficient data gives the values of β, listed in Table 4. For this model, the estimates of Ce^{4+} fraction equal to p/N increase in air from 24 to 27% when x increases from 0 to 0.2. The calcium charge compensation is thus predicted to occur *via* decreasing oxygen hyperstoichiometry; the corresponding δ values calculated by eqn. (1) decrease from 0.12–0.13 ($x = 0$) down to 0.0075–0.0076 ($x = 0.2$).

The second model (Model 2) is similar to Model 1, but the transported heat of holes was neglected.[34,37] In this case, the temperature dependence of the Seebeck coefficient is determined by the variations in charge carrier concentration. For this model, the values of y at 923–1223 K in air were estimated as 0.08–0.11, 0.23–0.24 and 0.25–0.26 for $x = 0$, 0.1 and 0.2, respectively. The charge compensation is, hence, *via* the hole generation at small calcium additions and *via* decreasing oxygen hyperstoichiometry at larger x; the estimates of δ in air vary in the range 0.04–0.07, 0.05–0.06 and 0.002–0.004 at $x = 0$, 0.1 and 0.2, correspondingly. For $x = 0$–0.1, these values are quite close to those estimated from the structure refinement results (Table 2).

Both these simplified models provide only qualitative agreement with the data on ionic conductivity and structure of $Ce_{1-x}Ca_xVO_{4+\delta}$, but confirm the non-negligible presence of Ce^{4+} and oxygen interstitials. The estimates of the point defect concentrations obtained using Model 2 are considered as more adequate. In particular, the existence of about 25% Ce^{4+} in the lattice of $CeVO_{4+\delta}$ in air, given by Model 1, contradicts the X-ray absorption spectroscopic data, whilst the small fraction of Ce^{4+} (4–7%) predicted by Model 2 may be reflected by a small shoulder at 5730–5745 eV in the XAS spectra.[9]

3.7. Electron-hole mobility

Although the estimations obtained by the simplest hopping models agree with the experimental data only qualitatively, the results do suggest a small-polaron mechanism of the p-type conduction. This mechanism was further supported by the data

Table 4 Electron-hole mobility and its activation energy for $Ce_{1-x}Ca_xVO_{4+\delta}$ in air[a]

		E_a/kJ mol^{-1}		ln μ_0/cm^2 K V^{-1} s^{-1}		β	
X	T/K	Model 1	Model 2	Model 1	Model 2	Model 1	Model 2 (1073 K)
0	1023–1173	44 ± 4	27 ± 2	2.3 ± 0.4	1.4 ± 0.2	3.5 ± 0.2	2.54 ± 0.05
0.1	1023–1223	36 ± 1	35 ± 1	3.4 ± 0.1	3.3 ± 0.1	3.58 ± 0.01	3.40 ± 0.07
0.2	1023–1173	41 ± 4	40 ± 4	4.3 ± 0.4	4.3 ± 0.4	3.61 ± 0.01	3.54 ± 0.07

[a] E_a and μ_0 are the regression parameters of Arrhenius model for the temperature dependence of electron-hole mobility, $\mu \times T = \mu_0 \times \exp(-E_a/RT)$.

on p-type carrier mobility. By definition, the mobility (μ) is related to the conductivity as

$$\mu = \frac{\sigma}{ep} \quad (5)$$

where the charge carrier concentration (p) can be calculated from the p/N ratio, estimated from the Seebeck coefficient data. The values of N, equal to the total concentration of cerium sites, were determined from XRD results (Table 2).

The estimations of the electron-hole mobility in air are presented in ESI and Table 4. As for the p-type conductivity, the mobility has a temperature-activated character, with an activation energy of 27–44 kJ mol^{-1}. Although $p(O_2)$ variations induce obvious changes in the charge carrier concentration (Figs. 4 and 5), the hole mobility is essentially independent of the oxygen pressure (see ESI), as expected. The values of μ, estimated by Models 1 and 2, are quite similar. The magnitudes of the hole mobility in $Ce_{1-x}Ca_xVO_{4+\delta}$, which varies in the range (0.6–12) $\times$ 10^{-4} cm^2 V^{-1} s^{-1} at 923–1223 K, and the corresponding activation energy values (Table 4) are both characteristic of small-polaron conductors.

4. Conclusions

Single-phase ceramics of zircon-type $Ce_{1-x}A_xVO_4$ (A = Ca, Sr; x = 0–0.2) with density higher than 93% were studied using XRD, dilatometry, and measurements of the total electrical conductivity, faradaic efficiency and Seebeck coefficient at 300–1300 K in the oxygen partial pressure range from 10^{-19} to 0.75 atm. The average thermal expansion coefficients of $Ce(A)VO_4$ in air are (5.6–5.9) $\times$ 10^{-6} K^{-1} at 400–800 K. Substitution of cerium with alkaline-earth cations leads to increasing total conductivity, predominantly p-type electronic, and to a change in the sign of the Seebeck coefficient due to increasing electron-hole concentration. The activation energy for p-type conduction varies in the range 34–38 kJ mol^{-1}; the low hole mobility values are typical for a small-polaron conduction mechanism. TGA studies showed that within the zircon phase stability limits, the total oxygen content variations in the studied range of temperature and oxygen partial pressure are minor, less than 1–2%, which results in weak $p(O_2)$ dependences of the electrical properties. Calculations of the p-type charge carrier concentration suggest the presence of Ce^{4+} cations and hyperstoichiometric oxygen ions. The formation of tetravalent cerium is responsible for decreasing unit cell volume and increasing p-type conductivity when x increases. Doping with calcium was found to considerably enhance the stability of zircon-type cerium vanadate at reduced oxygen pressures. The oxygen ion transference numbers of $Ce_{1-x}Ca_xVO_{4+\delta}$ in air, determined by the faradaic efficiency measurements, are in the range from 2 $\times$ 10^{-4} to 6 $\times$ 10^{-3} at 973–1223 K. The ionic conductivity decreases with reducing oxygen pressure and has similar values for $CeVO_{4+\delta}$ and $Ce_{0.8}Ca_{0.2}VO_{4+\delta}$, indicating an interstitial diffusion mechanism, which confirms oxygen hyperstoichiometry of the cerium vanadate-based phases.

Acknowledgements

This research was partially supported by the FCT, Portugal (PRAXIS and POCTI programs and project BD/6827/2001), Commission of the Russian Academy of Sciences for Young Scientists Support (6th competition, grant 192), and the Belarus Ministry of Education and Science. The authors are sincerely grateful to Ilia Leonidov for helpful discussions and Alexandre Shaulo for experimental assistance.

References

1 U. O. Krasovec, B. Orel and R. Reisfeld, *Electrochem. Solid State Lett.*, 1998, **1**, 104.
2 A. M. Salvi, F. Decker, F. Varsano and G. Speranza, *Surf. Interface Anal.*, 2001, **31**, 255.
3 R. Cousin, D. Courcot, E. Aad Abi, S. Capelle, J. P. Amoureux, M. Dourbin, M. Guelton and A. Aboukais, *Colloid. Surf. A*, 1999, **158**, 43.
4 J. Matta, D. Courcot, E. Aad Abi and A. Aboukais, in *Environment and Solar, Proc. 2000 Mediterranean Conf.*, IEEE, Piscataway, NJ, 2001, p. 278.
5 K. Gaur and H. B. Lal, *J. Mater. Sci.*, 1985, **20**, 3167.
6 H. C. Nguyen and J. B. Goodenough, *J. Solid State Chem.*, 1995, **119**, 24.
7 A. Watanabe, *J. Solid State Chem.*, 2000, **153**, 174.
8 T. Hirata and A. Watanabe, *J. Solid State Chem.*, 2001, **158**, 254.
9 R. F. Reidy and K. E. Swider, *J. Am. Ceram. Soc.*, 1995, **78**, 1121.
10 K. Gaur and H. B. Lal, *J. Mater. Sci.*, 1985, **20**, 3167.
11 S. Pizzini, C. M. Mari and L. Zanderighi, *Gazz. Chim. Ital.*, 1976, **106**, 299.
12 C. M. Mari, *Solid State Ionics*, 1984, **12**, 419.
13 H. Uchida, H. Suzuki and M. Watanabe, *J. Electrochem. Soc.*, 1998, **145**, 615.
14 S. Primdahl, J. R. Hansen, L. Grahl-Madsen and P. H. Larsen, *J. Electrochem. Soc.*, 2001, **148**, A74.
15 V. V. Kharton, F. M. Figueiredo, L. Navarro, E. N. Naumovich, A. V. Kovalevsky, A. A. Yaremchenko, A. P. Viskup, A. Carneiro, F. M. B. Marques and J. R. Frade, *J. Mater. Sci.*, 2001, **36**, 1105.
16 Yu. D. Tretiakov, *Chemistry of Nonstoichiometric Oxides*, Moscow State University, Moscow, 1974.
17 H. Yokokawa, N. Sakai, T. Kawada and M. Dokiya, *Solid State Ionics*, 1992, **52**, 43.
18 J. Rodriguez-Carvajal, *Physica B*, 1993, **192**, 55.
19 V. V. Kharton, A. V. Kovalevsky, A. P. Viskup, F. M. Figueiredo, A. A. Yaremchenko, E. N. Naumovich and F. M. B. Marques, *J. Electrochem. Soc.*, 2000, **147**, 2814.
20 V. V. Kharton, A. P. Viskup, F. M. Figueiredo, E. N. Naumovich, A. A. Yaremchenko and F. M. B. Marques, *Electrochim. Acta*, 2001, **46**, 2879.
21 V. V. Kharton, A. P. Viskup, A. V. Kovalevsky, F. M. Figueiredo, J. R. Jurado, A. A. Yaremchenko, E. N. Naumovich and J. R. Frade, *J. Mater. Chem.*, 2000, **10**, 1161.
22 I. A. Leonidov, V. L. Kozhevnikov, E. B. Mitberg, M. V. Patrakeev, V. V. Kharton and F. M. B. Marques, *J. Mater. Chem.*, 2001, **11**, 1202.
23 E. B. Mitberg, M. V. Patrakeev, A. A. Lakhtin, I. A. Leonidov, V. L. Kozhevnikov and K. R. Poeppelmeier, *J. Alloys Compd.*, 1998, **274**, 103.
24 D. P. Fagg, J. C. Waerenborgh, V. V. Kharton and J. R. Frade, *Solid State Ionics*, 2002, **146**, 87.
25 H. Hayashi, M. Suzuki and H. Inaba, *Solid State Ionics*, 2000, **128**, 131.
26 R. D. Shannon, *Acta Crystallogr., Sect. A*, 1976, **32**, 751.
27 L.-P. Li, G.-S. Li, Y.-F. Xue and H. Inomata, *J. Electrochem. Soc.*, 2001, **148**, J45.
28 V. V. Kharton, A. P. Viskup, E. N. Naumovich and F. M. B. Marques, *J. Mater. Chem.*, 1999, **9**, 2623.
29 *Phase Equilibria Diagrams. CD-Rom Database*, ed. P. Schenck, The American Ceramic Society, Westerville, OH, 1998.
30 I. A. Leonidov, A. A. Fotiev and M. Ya. Khodos, *Inorg. Mater.*, 1987, **23**, 107.
31 G. H. Jonker, *Philips Res. Rep.*, 1968, **23**, 131.
32 P. Kofstad, *Nonstoichiometry, Diffusion and Electrical Conductivity in Binary Metal Oxides*, Wiley-Interscience, New York, 1972.
33 V. N. Chebotin, *Physical Chemistry of Solids*, Khimiya, Moscow, 1982.
34 J. Nell, B. J. Wood, S. E. Dorris and T. O. Mason, *J. Solid State Chem.*, 1989, **32**, 247.
35 M. S. Seltzer and A. Z. Hed, *J. Electrochem. Soc.*, 1970, **117**, 815.
36 K. Kobayashi, S. Yamaguchi, T. Tsunoda and Y. Imai, *Solid State Ionics*, 2001, **144**, 123.
37 J. B. Goodenough, in *Conduction in Low-Mobility Materials*, ed. N. Klein, D. S. Tannhauser and M. Pollak, Taylor and Francis, London, 1971, p. 87.
38 Z. S. El Mandough and M. S. Selim, *Thin Solid Films*, 2000, **371**, 259.